AFRL-AFOSR-UK-TR-2013-0007

Transition Control with Dielectric Barrier Discharge Plasmas

Professor Cameron Tropea

Technisch Universitaet Darmstadt
Petersenstrasse 30
Darmstadt 64287 Germany

EOARD Grant 11-3067

Report Date: January 2013

Final Report from 01 October 2011 to 30 September 2012

Air Force Research Laboratory
Air Force Office of Scientific Research
European Office of Aerospace Research and Development
Unit 4515 Box 14, APO AE 09421

REPORT DOCUMENTATION PAGE

Form Approved OMB No. 0704-0188

1. REPORT DATE *(DD-MM-YYYY)*	2. REPORT TYPE	3. DATES COVERED *(From – To)*
3 January 2013	Final Report	1 October 2011 – 30 September 2012

4. TITLE AND SUBTITLE

Transition Control with Dielectric Barrier Discharge Plasmas

5a. CONTRACT NUMBER

FA8655-11-1-3067

5b. GRANT NUMBER

Grant 11-3067

5c. PROGRAM ELEMENT NUMBER

61102F

6. AUTHOR(S)

Professor Cameron Tropea

5d. PROJECT NUMBER

5d. TASK NUMBER

5e. WORK UNIT NUMBER

7. PERFORMING ORGANIZATION NAME(S) AND ADDRESS(ES)

Technisch Universitaet Darmstadt
Petersenstrasse 30
Darmstadt 64287 Germany

8. PERFORMING ORGANIZATION REPORT NUMBER

N/A

9. SPONSORING/MONITORING AGENCY NAME(S) AND ADDRESS(ES)

EOARD
Unit 4515 BOX 14
APO AE 09421

10. SPONSOR/MONITOR'S ACRONYM(S)

AFRL/AFOSR/IOE (EOARD)

11. SPONSOR/MONITOR'S REPORT NUMBER(S)

AFRL-AFOSR-UK-TR-2013-0007

12. DISTRIBUTION/AVAILABILITY STATEMENT

Approved for public release; distribution is unlimited.

13. SUPPLEMENTARY NOTES

14. ABSTRACT

Two experimental setups have been employed to foster the understanding of DBD transition control mechanisms and to optimize the obtainable transition delay on a flat plate and on a wing glove for flight investigations. Accompanying numerical investigations support the experimental findings and enable parametrical studies for optimization purposes. Generic flat-plate wind-tunnel experiments demonstrate the control of naturally occurring,TS-wave dominated transition by means of a single DBD actuator. A parametric variation of the actuator number, thrust and positioning indicates a strong dependence of the transition control effectiveness on all these parameters. Increased effectiveness is found for higher forcing magnitudes; however, no flow control optimum is identified at the selected speed of $U\infty$ = 20 m/s. The limited momentum induced by the single actuator compared to the freestream momentum restricts the obtainable effect. Due to the danger of dielectric breakdown at excessively high voltages, a limitation of the actuator power is necessary, such that the best achievable transition delay is limited by the actuator performance and not by stability effects. A variation of the actuator position and application of multiple-actuator arrays yields significantly enhanced effectiveness for optimized locations. The conducted experiments insinuate that adequate positioning of an actuator is more important than a multiplication of the force locations which provokes a increase of the total power consumption. Initial wind-tunnel measurements and following flight tests with a specially designed wing glove demonstrate the possibility to delay naturally occurring transition by means of steadily operated DBD actuators at Re = 3 × 106 under varying ambient conditions. The atmospheric conditions and their influence on the DBD power consumption have been thoroughly analyzed, paving the way for a successful implementation of a closed-loop performance controller and enabling constant flow-control authority during measurement flights. Although the presented effort is not the very first airborne DBD application, compare [15], it is the first and only one to show a desirable flow-control effect under realistic flight conditions. The respectable transition delay of 3% chord length during the first non-optimized flights agrees with initial wind-tunnel measurements and exceeds the expectations from numerical simulations. Both the numerics and the flight experiments indicate a saturation of the control effectiveness despite increasing thrust magnitude, such that an efficiency consideration between the energy expense and savings is necessary. A conservative calculation of the net drag reduction by approximately 1.9% results in a computed power efficiency in the two-digit percentage range, rendering a net benefit plausible if the experimental setup is refined and further optimized

15. SUBJECT TERMS

EOARD, Plasma Aerodynamic, transition control, Dielectric Barrier

16. SECURITY CLASSIFICATION OF:			17. LIMITATION OF ABSTRACT	18, NUMBER OF PAGES	19a. NAME OF RESPONSIBLE PERSON
a. REPORT	b. ABSTRACT	c. THIS PAGE			Gregg Abate
UNCLAS	UNCLAS	UNCLAS	SAR	28	19b. TELEPHONE NUMBER *(Include area code)* +44 (0)1895 616021

Transition Control with Dielectric Barrier Discharge Plasmas

Dipl.-Ing. A. Duchmann
Dr.-Ing. S. Grundmann
Prof. Dr.-Ing. C. Tropea

TECHNISCHE UNIVERSITÄT DARMSTADT

CSI

End of Grant Report

Award No. FA8655-11-1-3067

Abstract

The objective of the project is to control natural boundary-layer transition through the use of dielectric barrier discharge (DBD) plasma actuators. Transition delay or even suppression has its merits not only in lower wall shear stress and frictional drag of laminar as opposed to turbulent boundary layers, but transition control can be instrumental in influencing flow separation, which opens avenues for significantly influencing pressure drag and wake acoustics of bluff bodies or profiles.

The focus of the project is on understanding fundamentals of the transition control with DBD actuators and on optimization of actuator design and operating parameters. The project is of experimental nature with accompanying numerical studies. The main questions to be answered concern the applicability of plasma actuators for delay of naturally occurring boundary-layer transition at elevated Reynolds numbers and the characterization of the relevant physical effects. For the understanding of the stabilizing effect, a generic flat plate experiment is used whereas transition delay at elevated Reynolds numbers is demonstrated during in-flight experiments on a motorized glider.

Contents

1 Introduction

An earlier project funded by AFOSR ([1], Grant FA8655-08-1-3032) aimed at a better understanding of transition control with dielectric barrier discharge (DBD) plasma actuators as well as their working principles in quiescent air and laminar boundary layers. Enhanced DBD actuator configurations were investigated for laminar boundary-layer flow control, including the so called 'Sliding Discharge'-technology. The hydrodynamically stabilizing effect of the plasma force field was analyzed in comparison to standard DBD setups which have been used by several authors to obtain a delay of boundary-layer transition [14, 9, 16].

The final objective of the current project is to bring DBD actuators to free-flight application. In order to conduct boundary-layer control on a Grob G109 aircraft, a special wing glove was designed, built, tested and instrumented during the two years of the former project. First wind-tunnel tests demonstrated promising conditions for DBD transition delay, paving the way for transition experiments at elevated Reynolds numbers in the present project.

A final goal of the project being the application of DBD actuators in free-flight, the high encountered free-stream velocities under such conditions pose a difficult environment for DBD flow control. The higher the bulk flow velocity, the lower is the ratio of the actuator's momentum input compared to the energy contained in the surrounding fluid, thus reducing the absolute flow control authority. Accurate positioning of DBD actuators is necessary to optimize the desired transition delay. A parametric study of position and thrust variations was therefore performed on a generic flat plate wind tunnel setup to find the most suitable configuration for DBD transition delay and analyze the stability properties of the manipulated flow. Such flow-control optimization can best be performed by numerical studies which accompany the experimental approach.

As in the earlier AFOSR-funded project, two ways of DBD transition control are pursued: the stabilization of laminar boundary-layer flow by continuous addition of momentum as well as the active cancelation of Tollmien-Schlichting instabilities. Both approaches have successfully been applied on generic flat plate setups in wind tunnels [9] and are applied at higher Reynolds numbers in the present study. Although promising results have been obtained by active wave cancelation during the course of the project, this report focusses on the effect of boundary-layer stabilization by continuous actuator operation at higher Reynolds numbers. These higher Reynolds numbers are obtained by increasing the model size and the flow velocities. For a realistic application, a wing glove is installed in the large NWK wind tunnel and tested under flight conditions on a G109b motorized glider.

2 Generic Flat Plate Setup

For increased effectiveness of DBD flow control, an optimization of the obtainable transition delay is desired. Earlier investigations by [9] on a flat plate demonstrated enhanced transition delay by increasing the actuator thrust and changing the actuator location. By systematic variation of both parameters, the dependence between actuator forcing and the flow stability properties is explored and conclusions concerning the flow-control effectiveness are drawn. Controlled experiments are conducted on a flat plate at $U = 20\,\mathrm{m/s}$ in a $450 \times 450\,\mathrm{mm}^2$ test section of an open-loop wind tunnel. Details on the experimental apparatus are reviewed in [1]. An adverse pressure gradient is created by shaping of the wind-tunnel walls to provoke natural laminar-turbulent transition by amplification of Tollmien-Schlichting instabilities within the test section. The same setup was used for PIV investigations of the DBD effect on discrete Tollmien-Schlichting instabilities presented in [6].

2.1 Thrust Variation

First, a single DBD actuator is positioned $x = 350\,\mathrm{mm}$ downstream of the leading edge. It extends across the full spanwise dimension of the flat plate (450 mm) and is composed of copper electrodes and Kapton dielectric of 0.3 mm thickness. A *MiniPuls 2.1* high-voltage generator is used to operate the plasma actuator. The actuator thrust T, which is linearly related to the power consumption P of a specific actuator configuration [11], is varied to evaluate the influence on the transition delay. By systematically increasing the supply voltage V_{pp}, the power consumption P and subsequently the thrust T imposed on the surrounding fluid increases.

The standard deviation of a hot-wire signal traversed along the streamwise direction is utilized to quantify the transition location as illustrated in Figure 2.1. The transition location without DBD forcing (solid line) is resembled by the signal peak at $x = 0.52\,\mathrm{m}$. DBD operation at $V_{pp} = 6\,\mathrm{kV}$ and $T = 7.8\,\mathrm{mN/m}$ provides a homogeneous surface discharge but only a small delay

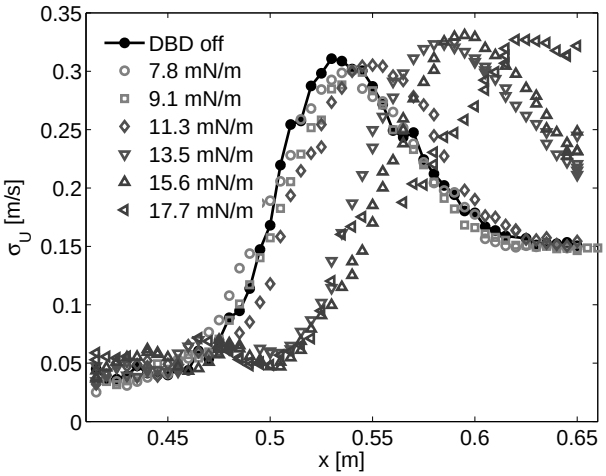

Figure 2.1: Velocity standard deviation σ_U along flat plate as a function of actuator thrust T.

of transition is observed. For higher applied body forces, the transition delay effect is enhanced, but care has to be taken not to exceed the breakdown voltage which destroys the actuator. A downstream shift of the transition location in the range of $10 - 95$ mm is obtained by varying the integral actuator thrust between 7.8 mN/m and 17.7 mN/m. Grundmann [9] proposed the existence of an optimum body force for transition delay at much lower flow velocities between $U_\infty = 6 - 8$ m/s. At the present flow speed and with the given actuator materials, no optimum can be identified due to breakdown-voltage limitations. Yet it remains promising to increase the DBD thrust if adequate dielectric materials (e.g. ceramics) are available, especially if flow control at even higher freestream velocities is attempted. Presently, it appears more promising to apply multiple consecutive actuator arrays with lower individual force magnitudes in the linear amplification range of Tollmien-Schlichting instabilities.

2.2 Actuator Arrays

After thorough analysis of the transition behavior influenced by a single DBD actuator at a fixed location, the actuator position is focussed to enhance the transition control effectiveness. Besides the position of a single actuator, arrays of actuators consecutively placed in streamwise direction promise a more homogeneous flow forcing at reduced force magnitude levels.

Three identical DBD actuators are flush-mounted on the flat plate at different locations $x_1 = 320$ mm, $x_2 = 350$ mm and $x_3 = 380$ mm. They can be operated independently or in combination at any desired thrust. The DBD operating frequency $f_{pl} = 6$ kHz is kept constant to facilitate the comparison with the single-actuator experiments at $x = x_2 = 350$ mm. The integral thrust is maintained at an intermediate level of $T = 15.6$ mN/m to avoid premature actuator damage and obtain a relatively large transition delay. In the case of multiple actuator arrays, the net actuator length increases and the total consumed power is multiplied by the number of actuators.

First, the DBD actuators are operated independently at various locations to evaluate the effect of positioning on the transition delay. Figure 2.2 illustrates the hot-wire standard deviation along the flat plate for DBD operation at the three positions $x_1 - x_3$. At x_1, almost no transition

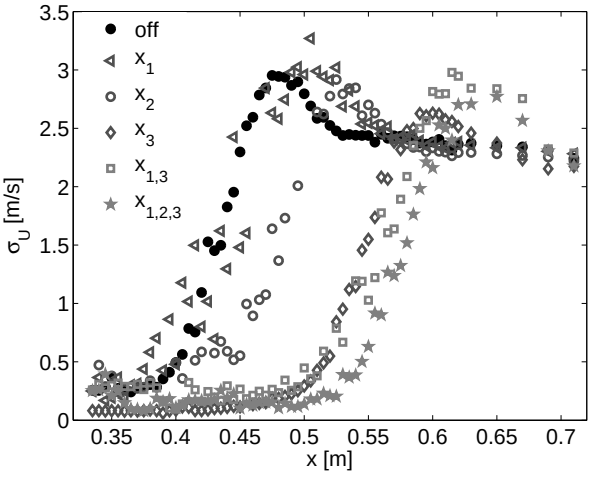

Figure 2.2: Transition positions as a function of actuator placement and array permutation, $T = 15.6$ mN/m, $U_\infty = 20$ m/s.

delay is observed whereas DBD forcing at x_2 approximately confirms the $\Delta x_{\text{trans}} = 55$ mm found the results in the preceding section. The slightly reduced $\Delta x_{\text{trans}} = 50$ mm might derive from subtle variations of the wind-tunnel conditions. If operated at x_3, the transition is significantly postponed, yielding $\Delta x_{\text{trans}} = 120$ mm. If the first and last actuator are operated together ($x_{1,3}$), the additional improvement of the transition delay is marginal, $\Delta x_{\text{trans}} = 140$ mm, in comparison to separate operation of the third actuator. By adding the remaining actuator ($x_{1,2,3}$), another 25 mm are gained to $x_{\text{trans}} = 165$ mm.

In context of position variation of single DBD actuators, the placement at the farthest downstream position x_3 is most effective to delay transition. Following this trend, the existence of an optimum location can be expected since the actuator will not be effective if positioned beyond the natural transition location. Further downstream placements would have required complex modifications of the test rig, such that no optimum location is identified. If other actuators are added, only slight improvements are measured at the cost of doubled or tripled power consumption. In terms of efficiency, relating the net effect to the energy expenditure, operation of all three actuators at the same power consumption cannot be recommended although the effectiveness is enhanced. Adaption of the actuator magnitude according to the respective position may be a final necessity to optimize the flow-control efficiency. Nevertheless, the presented results indicate that correct actuator positioning is of higher importance for increasing the overall transition-delay effectiveness on a flat plate.

2.3 Numerical Studies

Linear stability analysis [5] of experimental and numerical data as presented in [7] is useful to evaluate the stabilizing influence on different setups. Tollmien-Schlichting wave amplitudes are represented by the normalized N-factor N and provided in Figure 2.3 (a) for the case without DBB actuation. In agreement with an empirical law by Mack [13] relating the turbulence intensity of the wind tunnel flow to the transitional N-factor, transition is expected to occur in the vicinity of $x = 0.48$ m based on a most unstable frequency of 380 Hz. The effect of the local stabilization due to DBD operation by a single DBD actuator is illustrated in Figure 2.3 (b). The N-factor downstream of the actuator location $x = 0.35$ m is significantly reduced for all disturbance frequencies. The disturbance amplitudes start to grow again a few millimeters downstream, but the location of crossing the transition threshold is moved to $x = 0.54$ m. This shift of the threshold location of approximately 55 mm downstream agrees well with the experimentally measured transition delay for a single DBD at $x = x_2$ in the former sections. Additionally, the stability analysis reveals that the frequency relevant for transition is shifted towards lower values, here to approximately $f = 320$ Hz. The numerical stability analysis confirms the stabilizing effect of the DBD actuator, such that the main mechanism for the transition delay is explained by a change of the hydrodynamic stability properties of the flow due to the actuator forcing. More comparisons between experiments and numerical investigations are found in [8].

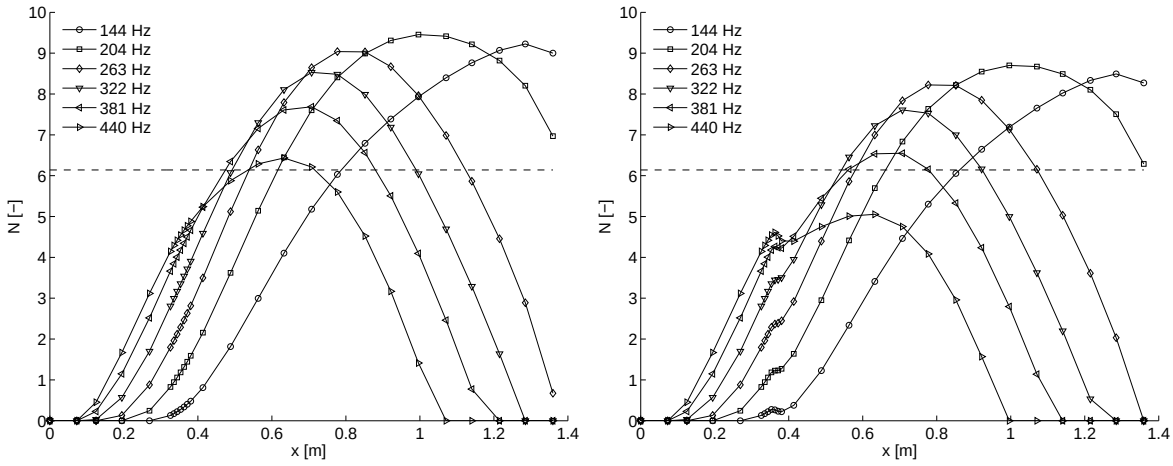

(a) DBD off (b) $T = 11$ mN/m

Figure 2.3: N-factor evolution for discrete disturbance frequencies (various markers) without (a) and with (b) DBD actuation at $T = 11.3$ mN/m.

3 Wing Glove Experiments

The G109b motorized glider plane operated by the Institute of Fluid Mechanics and Aerodynamics at Technische Universität Darmstadt is an ideal platform for transition experiments under realistic flight conditions. The project plan stipulates in-flight experiments on DBD based transition control. Since such experiments need long-term preparations and acquisition of specialized hardware, work on the experimental apparatus had already been initiated during the first AFOSR-funded project [1]. In order to convey the DBD experiments to the in-flight environment, a special wing glove is built. This device covers part of the original glider wing and provides space and surface for implementation of experimental equipment.

The wing glove is made of epoxy-resin reinforced glass- and coal-fibres and can either be applied on the glider wing or on a special support in the *NWK* wind tunnel at TU Darmstadt. The sensors on the wing glove include 64 pressure taps distributed along the chord to measure the pressure distribution. Initial pressure distribution measurements presented in the final project report of the earlier AFOSR-Grant [1] indicated almost linear pressure gradients on the glove pressure side. Since the pressure gradient magnitude can be adjusted by varying the angle of attack, the pressure side was chosen for the systematic flow control experiments.

Exchangeable acrylic inserts in the center portions of the pressure and suction sides of the wing glove can be instrumented according to the specific experimental needs. For the transition delay experiments, a streamwise row of 15 *Sennheiser KE 4-211-2* microphones is installed underneath the surface, connected to the flow by 0.2 mm diameter orifices. The microphones are evenly distributed with 30 mm spacing between $x/c = 0.36$ and $x/c = 0.67$ and the signals are conducted to a self-built amplifier, enabling a resolution of the boundary-layer instability frequencies as well as the characterization of the transition location.

Boundary-layer measurements along the wing-glove surface are crucial to determine the state of the transitional boundary layer and measure the shape and amplitudes of contained disturbances. In order to acquire time-resolved velocity data along the exchangeable plexiglas measurement insert, a light-weight three-axis traversing system was developed which can be installed on either side of the wing glove. A sketch of the traversing system is provided in Figure 3.1 (a), indicating the single components with different colors. Two turrets (grey) are connected to variable mounting threads along the glove chord to both sides of the measurement insert. Both turret heads provide coaxial pivot points on which a linear traversing assembly for the spanwise direction (blue) is supported. On the moving sledge of this linear traverse, another linear traverse (green) is mounted enabling streamwise movement of a hot-wire probe support. The set of linear traverses may be rotated around the pivot point by a stepper motor positioned next to the inboard turret (red), leading to a wall-normal probe displacement with respect to the glove surface. The wall-normal positioning accuracy is 0.1 mm for highly resolved boundary-layer profiles. The lateral dimensions can be approached with approximately 1 mm accuracy. *NanoTech* stepper motors with feedback encoders ensure repeatability of the probe positioning.

Due to the convex nature of the wing glove and especially the non-monotonous curvature on the pressure side, the traverse kinematic illustrated in Figure 3.1 (b) has to account for non-linear movements by adequate software programming and stepper motor control. Small modifications of the hardware and sign changes within the relative coordinate systems are necessary

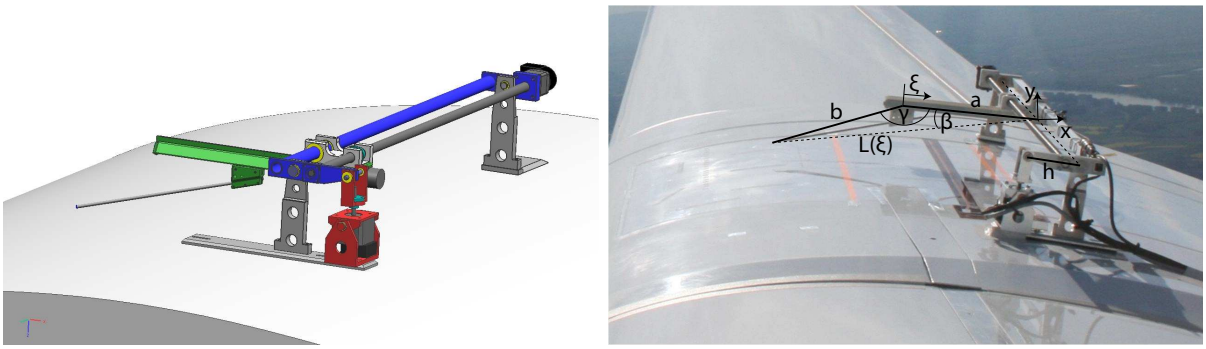

(a) Sketch of single traverse components for application on pressure side.

(b) Kinematic of the traverse system on the suction side during flight.

Figure 3.1: Sketch (a) and kinematic (b) of the traverse system for boundary-layer measurements on the wing glove.

when switching between pressure and suction side installation. The combination of linear and rotatory components creates a non-linear kinematic with mutual dependence of the positions of each stepper motor, requiring the definition of an absolute reference position. Boundary-layer velocity profiles can be acquired with a *Dantec 55P15* type hot-wire probe mounted to the 3D-traverse system and connected to a customized multi-channel *MiniCTA* Wheatstone bridge anemometer. The hot-wire equipment is calibrated to the expected flight speed via King's law and a temperature correction is applied. An overall sketch of the pressure side of the wing glove instrumented with the different sensors as well as further flight equipment is provided in Figure 3.2.

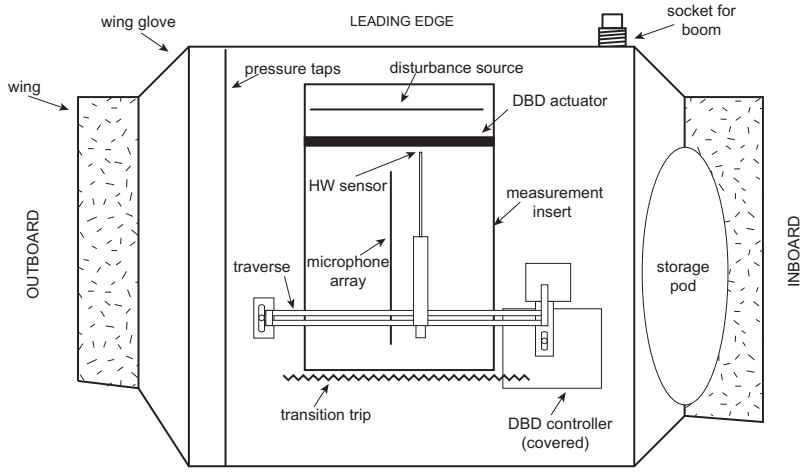

Figure 3.2: Overview of the wing glove pressure side with sensors and traverse system installed.

3.1 Wind Tunnel Experiments

In the 2×3 m *NWK* wind tunnel, the wing glove is mounted on a section of an original G109b wing which is vertically attached to the wind tunnel force balance as illustrated in Figure 3.3. The angle of attack can be arbitrarily traversed and the wind tunnel velocity raised up to 60 m/s such that flight reference conditions can be reproduced in the lab. Since it is difficult to cali-

brate the measurement equipment in flight, the possibility to account for these procedures and use the fully equipped in-flight setup in the wind tunnel is a beneficial advantage of the testing capabilities at Technische Universität Darmstadt. Additionally, the steady conditions of the wind tunnel flow facilitate the acquisition of the transition location and definition of a suitable configuration for transition delay experiments in flight.

Figure 3.3: Wing glove on support in *NWK* wind tunnel.

3.1.1 Identification of Adequate Transition Locations

To initiate successful flow-control measurements, the most promising flow conditions for transition experiments on the wing glove pressure side is sought for. Contrary demands pose an optimization problem; low flow speeds are desirable to retain a sufficient actuator effect due to limited thrust magnitudes. On the other hand, low velocities are associated with high angles of attack which lead to a very stable flow on the pressure side. A compromise has to be found to ensure hydrodynamic unstable flow and effective influence on transition locations accessible with the chosen measurement probes.

The transition process along an airfoil is most conveniently analyzed by varying the local Reynolds number $Re_x = U\,x/\nu$. This can be achieved by maintaining the flow speed U and evaluating sensor signals at several downstream locations x. If a quick overview over the general transition behavior is desired, measurements with distributed sensors at various positions in combination with a systematic change of the flow conditions are advantageous.

The flush-mounted microphone array in the center portion of the measurement insert monitors the level of velocity fluctuation associated with laminar-turbulent transition along the wing glove chord x/c. The contour levels in Figure 3.4 illustrate the streamwise evolution of the microphone signal standard deviation σ_M as the angle of attack is varied between $\alpha = -2.2°$ and

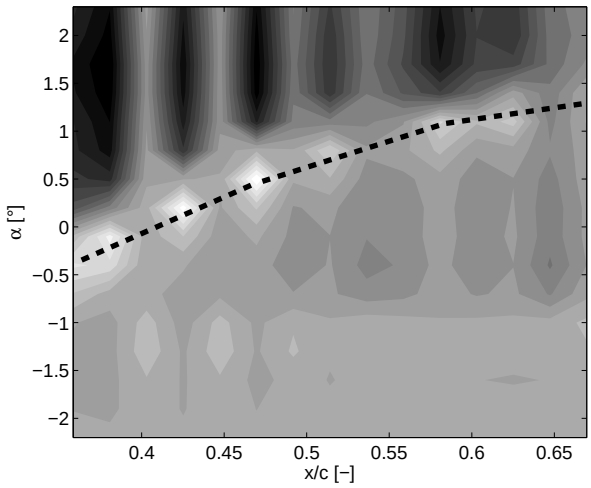

Figure 3.4: Microphone standard deviation related to the angle of attack.

2.3° for a constant flow velocity $U = 38\,\mathrm{m/s}$. Bright colors represent high fluctuation levels, indicative for the flow intermittency during laminar-turbulent transition. By maintaining a fixed velocity and changing the angle of attack of the model, the pressure gradient on the suction side is varied and the resulting displacement of the standard deviation peak is quantified. The dashed line, approximating the evolution of the maximum standard deviation, clearly shows that the transition location can be adjusted within the measurement region $x/c = 0.35 - 0.67$ for varying angles of attack $\alpha = -0.2 - -1.3°$. The initial parametric study yields an angle of attack of $\alpha = 0.7°$ as most promising to obtain the boundary-layer transition approximately in the center of the exchangeable measurement insert. For this design angle and the corresponding flow speed $U = 38\,\mathrm{m/s}$, maximum intermittency is obtained at $x/c = 0.51$ at the 8^{th} microphone position. The local Reynolds number at this position is $Re_x = 1.7 \times 10^6$.

The pressure distribution at $U = 38\,\mathrm{m/s}$ and varying angles of attack $\alpha = -0.2 - 1.3°$ is illustrated in Figure 3.5. The dimensionless pressure coefficient c_p along the streamwise chord position x/c characterizes the pressure gradients on the suction and pressure side of the wing glove. For $\alpha = -0.2°$, a strong positive gradient of $\mathrm{d}c_p/\mathrm{d}(x/c) = 0.23$ is found on the pressure side in the relevant region $x/c = 0.2 - 0.7$, indicating highly unstable conditions. Under such low angles of attack, transition is expected to occur close to the position of the DBD actuator at $x/c = 0.33$, and evidence can be found in Figure 3.4 through the microphone data. At the higher $\alpha = 1.3°$, the pressure gradient is approximately neutral ($\mathrm{d}c_p/\mathrm{d}(x/c) = 0.01$), leading to a much higher flow stability and postponed transition. For the design angle of attack $\alpha = 0.7°$, the dimensionless pressure gradient $\mathrm{d}c_p/\mathrm{d}(x/c) = 0.09$ is only slightly destabilizing the flow. Under such conditions, DBD flow control is effective for transition delay as shown in the following.

3.1.2 Quantification of Transition Delay

After having found an adequate setup such that transition occurs on the exchangeable acrylic insert and is measurable with the sensors, the transition control experiments are initiated. The primary objective of the following wind-tunnel tests is to identify DBD actuator configurations to effectively control the transition. A single DBD actuator is placed at $x/c = 0.33$ and extends

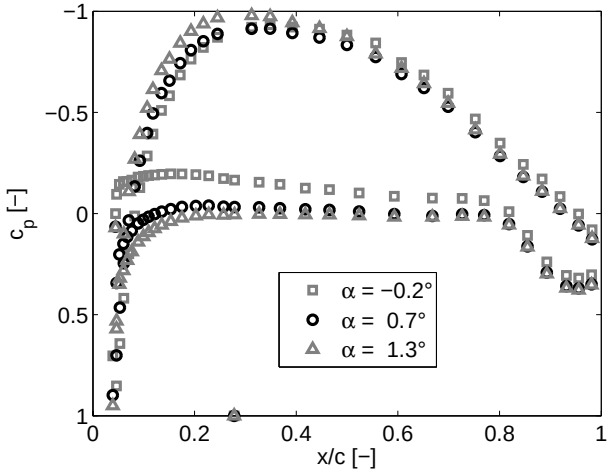

Figure 3.5: Dimensionless pressure distribution for varying angles of attack at constant speed $U = 38\,\mathrm{m/s}$.

600 mm in the spanwise direction. The actuator performance characteristics like thrust T and power consumption P are normalized with the actuator length to facilitate comparison to other experiments.

As expected, application of the single DBD plasma actuator leads to a downstream shift of the transition process. This can be quantified either by integral boundary-layer quantities like the shape factor H_{12} or the standard deviation of a sensor signal. All these values can be evaluated with a single hot-wire probe which is traversed with the 3-axis boundary-layer traverse. The hot wire enables acquisition of averaged boundary-layer velocity profiles as well as a statistical analysis of the anemometer signal. Figure 3.6 illustrates the effect of DBD actuation on the standard deviation σ_U of the velocity, acquired by a hot wire.

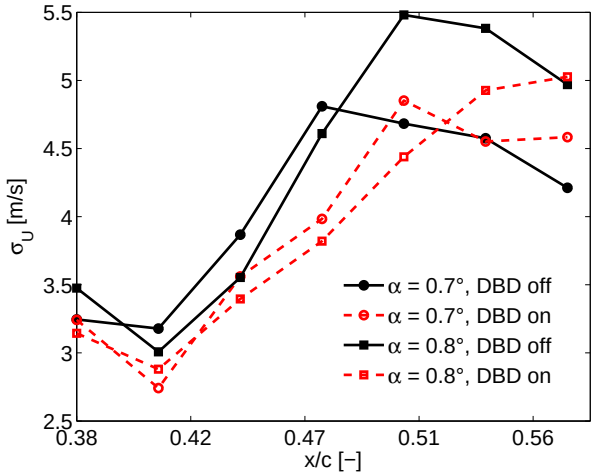

Figure 3.6: Standard deviation of hot-wire signal σ_U at the wall for various downstream locations x/c. The peaks indicate the maximum flow intermittency which is representative for the transition process.

The sensor is positioned at the wall ($y = 0\,\mathrm{mm}$) and traversed in streamwise direction x along the chord c. The peak of the signal fluctuation, encountered during maximum intermittency of the flow between the laminar and turbulent state, is found at $x/c = 0.47$ without DBD actuation for an angle of attack of $\alpha = 0.7°$ and slightly downstream ($x/c = 0.5$) for the less unstable $\alpha = 0.8°$. With DBD actuation, these positions are moved downstream, to $x/c = 0.5$ for $\alpha = 0.7°$ and even outside the observation region for $\alpha = 0.8°$. Although these results show a first and very successful delay of transition at large Reynolds numbers, measurement uncertainties impede an exact quantification of the actuator impact. Therefore, other quantities are investigated to validate the observations.

The shape factor H_{12} of the boundary-layer profile is illustrative for the transition process by combining the trends of the displacement thickness δ_1 and the momentum loss thickness δ_2. The shape factors of the same cases investigated before are illustrated in Figure 3.7, all showing a negative slope which is indicative for the ongoing transition. Despite data scatter and ambiguous detection of the wall position, the solid lines without DBD operation are set off from the dashed lines (indicating the flow-control cases). If the chord positions of two cases are evaluated for the same shape factor, e.g. $H_{12} = 1.8$, an offset by approximately $\Delta x/c = 0.03$ is observed. This value agrees quantitatively with the offset observed in the signal standard deviation in Figure 3.6.

The measured offset of both quantities translates into a physical transition delay of approximately $\Delta x_{\mathrm{trans}} = 40\,\mathrm{mm}$. The experiments are very successful considering the high freestream velocity and the pronounced adverse pressure gradient. The determined combination of angles of attack and flow speed is promising for further investigation in flight.

Despite high acoustic disturbances inside the wind-tunnel flow, a suitable setup and parameter range for flow-control experiments is identified. In the next step, the setup is mounted on the G109b glider wing to perform transition delay experiments in flight, based on the identified parameters. Before these measurements can be successfully performed, some constraints of in-flight experiments need to be addressed.

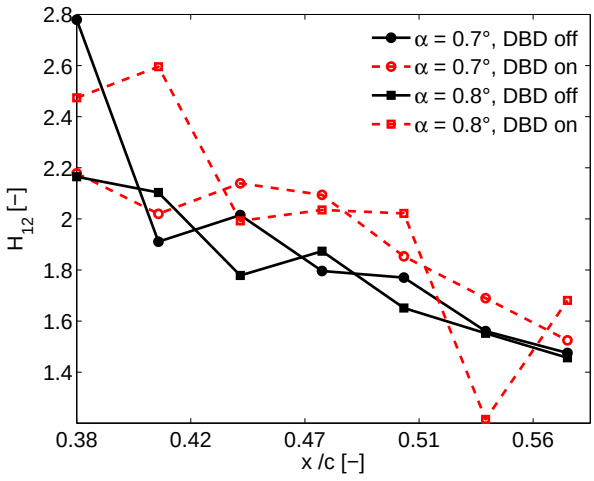

Figure 3.7: Shape factor H_{12} of the boundary layer as a function of the streamwise position x for two different angles of attack α.

3.2 In-Flight Experiments

3.2.1 Characterization of Ambient Condition Influences

Before the effect of DBD actuation on the flow can be quantified, the influence of the experimental conditions on the gas discharge requires consideration. A deterioration of DBD performance due to increasing flow velocities has been reported [12], and similar influences of pressure and humidity have been investigated [2, 3]. The ranges of the ambient conditions, including the flight speed encountered during the measurements, are summarized in Table 3.1. The table is

Altitude	A	$10'000$	-	0	ft
Pressure	p	0.7	-	1	bar
Density	ρ	0.86	-	1.3	kg/m^3
Temperature	t	-20	-	30	$°C$
Velocity	U_∞	20.3	-	44.5	m/s
Turbulence intensity	Tu	0.02	-	0.5	%
Relative humidity	h_{rel}	10	-	100	%

Table 3.1: Ambient conditions during measurement flights, divided into altitude dependent (top) and independent (bottom) quantities.

divided into parameters with dependence on the actual flight altitude and independent quantities. They will not be reviewed in detail but are exemplified by the ordering within the table. With decreasing altitude, the pressure, density and temperature increase. The remaining factors are not functionally related to the altitude but depend on the flight state and the weather.

Benard et al. [4] investigate the decrease of pressure, temperature and density associated with an altitude increase and identify the pressure to have the most prominent effect on DBD operation. With increasing altitude, the maximum velocities induced by a DBD actuator in

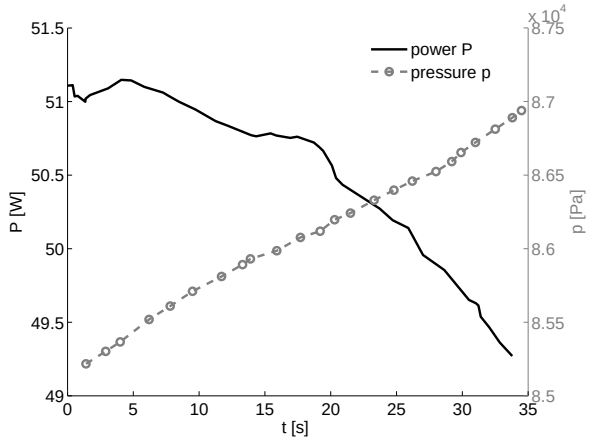

Figure 3.8: Power variation during pressure increase in gliding flight. The abscissa illustrates the measurement duration in seconds.

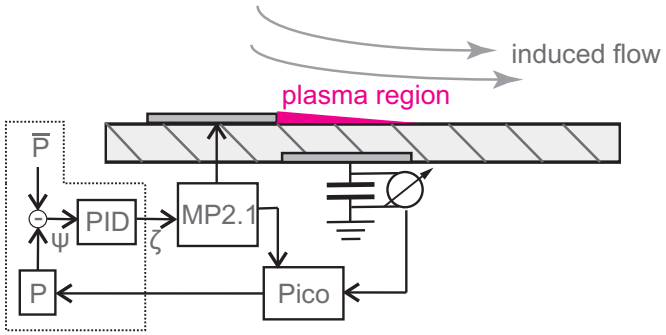

Figure 3.9: Sketch of the closed-loop power control setup including PID controller, *MiniPuls 2.1* (MP2.1) and *PicoScope* (Pico).

quiescent air are reduced. At the same time, the power consumption and extension of the plasma along the surface increase, mainly due to pressure effects.

The typical flight procedure for flow-control experiments is a motorless gliding descent starting from 10′000 ft altitude. The descent rate depends on the flight velocity chosen for the measurement, and the actual altitude is calculated from pressure measurements. Static pressure data are indicated in Figure 3.8 during a typical measurement flight, showing increasing pressure during the descent.

Additionally, the actuator power consumption is indicated for a constant supply voltage V_{pp}. The trend of decreasing power consumption with increasing pressure agrees well with the observations in [11, 4]. A 3% pressure increase leads to a 4% decrease of the consumed power, which is in agreement with observations by Kriegseis [11] who also reports a linear dependence. Besides the pressure, the humidity of the air is identified as an additional parameter to cause variations of the flow control performance. Especially in the vicinity of clouds, large humidity gradients can cause substantial DBD performance variations.

In order to maintain a constant flow control authority, a closed-loop algorithm for the actuator power consumption is developed. The *LabView* based real-time data acquisition facilitates the implementation of a control algorithm for the DBD performance. A feedback controller al-

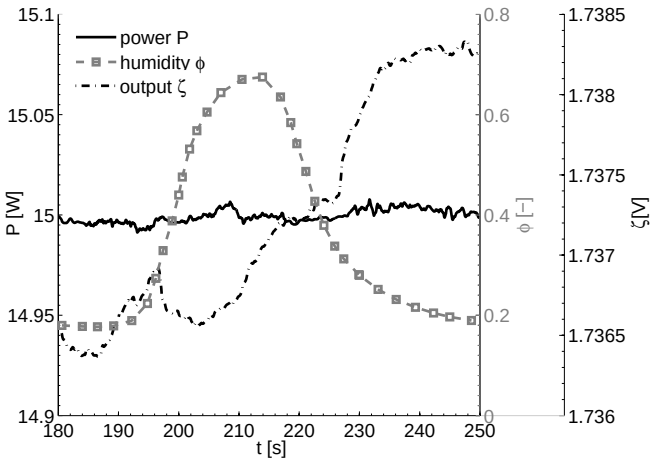

Figure 3.10: Closed-loop control of actuator power during humidity variation.

lows a comparison between the measured (P) and the target ($\bar{P}$) power value under any flight condition. The *National Instruments NI 9263* digital-analog output module closes the loop and sends a control signal ζ to the *MiniPuls 2.1* power supply to adjust the operating voltage. The principal setup of a closed-loop control circuit for the DBD power surveillance is illustrated in Figure 3.9.

A PID architecture was chosen for the software implementation of the control algorithm. Flight tests were performed to evaluate the operability of the power controller under varying conditions. Figure 3.10 illustrates measurements while crossing beneath a cloud base in motorized horizontal flight. The humidity increases significantly and the controller output is adjusted while maintaining the power constant at $P = \bar{P} = 15\,\mathrm{W}$.

During the following transition control experiments, the DBD actuator can be operated at constant performance despite varying ambient conditions.

3.2.2 Quantification of Transition Delay in Flight

In the following, measurements at a constant angle of attack of $\alpha = 0.7°$ at a flight speed of $U = 38\,\mathrm{m/s}$ are described while observing the microphone sensor signals at different downstream positions on the pressure side of the wing glove. The boundary-layer state can quickly be evaluated by considering the signal spectra. If the spectral amplitudes of frequencies f are visualized for each streamwise sensor position x/c in a contour level plot, Figure 3.11 is obtained. The ordinate shows the streamwise microphone positions whereas the frequencies are found on the abscissa. Red illustrates high amplitude levels whereas low amplitudes are blue. Without DBD operation, see Figure 3.11 (a), laminar flow is found at streamwise locations up to approximately $x/c = 0.47$, indicated by low disturbance amplitude levels. Only a confined range of higher amplitudes exists around $f = 600 - 800\,\mathrm{Hz}$, which represents the amplified Tollmien-Schlichting instabilities. A broadband increase of disturbance magnitudes associated

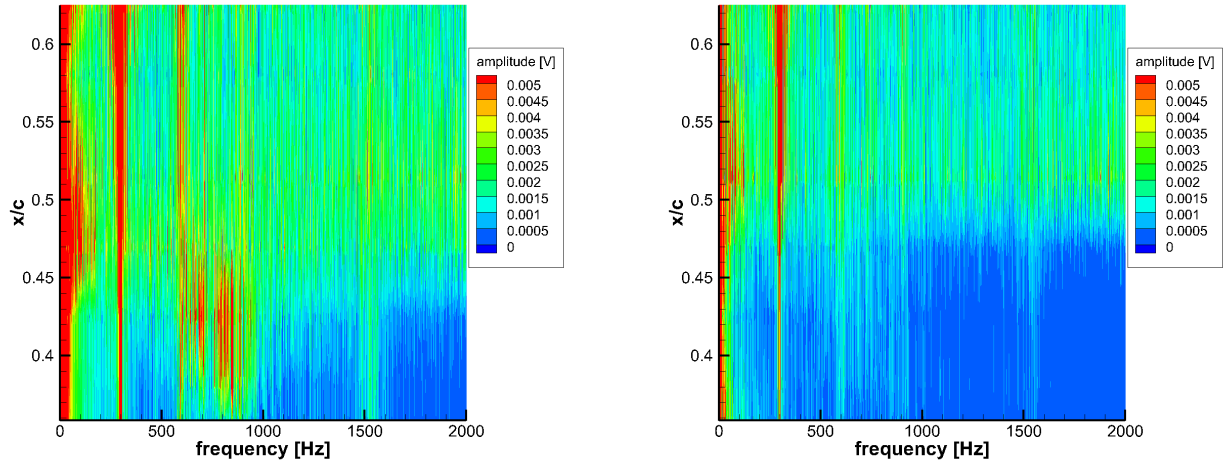

(a) DBD off (b) DBD on

Figure 3.11: Spectrogram of microphone signals for $\alpha = 0.7°$, traverse system installed, DBD on/off at $T = 16\,\mathrm{mN/m}$ ($P = 66.6\,\mathrm{W/m}$). Low signal amplitudes indicated in blue, high levels in red.

with transition to turbulence occurs downstream of $x/c = 0.47$. This transition location agrees well with the microphone measurements inside the wind tunnel. The effect of the single DBD actuator operated at controlled $P = 66.6\,\mathrm{W/m}$ and corresponding $T = 16.2\,\mathrm{mN/m}$ becomes apparent in Figure 3.11 (b). A delay of the transition by approximately 3% chord is indicated by further downstream occurrence of the broadband amplitude increase around $x/c = 0.5$. These results show the first successful DBD transition delay performed in flight under atmospheric conditions.

Additional measurements employing the hot-wire traverse yield similar transition delay results. The standard deviation of the hot-wire signal directly at the wall is measured along the downstream direction and illustrated in Figure 3.12. Again, a peak of the signal indicates the transition location. Measurements with activated flow control at $\alpha = 0.6°$, $U = 38.6\,\mathrm{m/s}$, shown

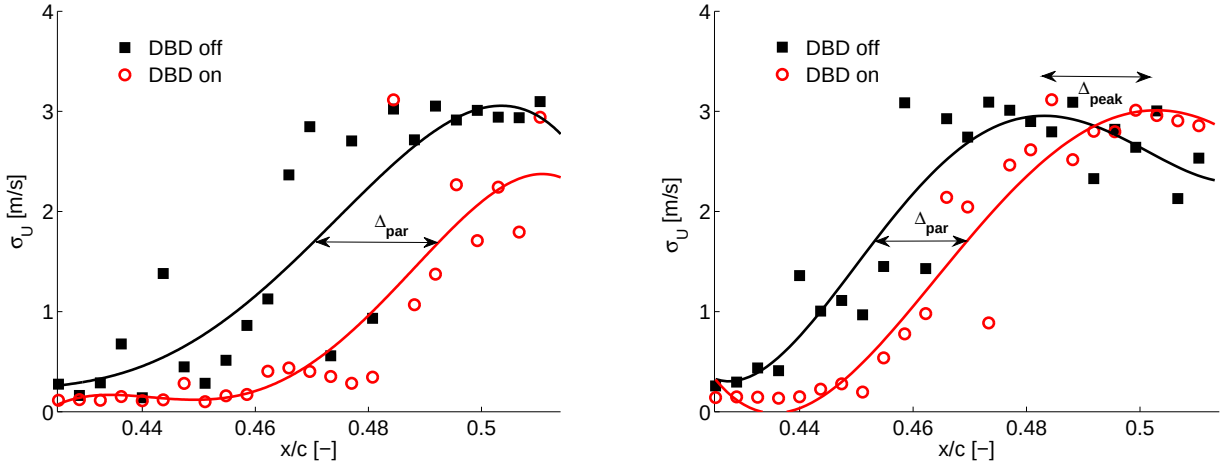

(a) $\alpha = 0.6°, U = 38.6\,\mathrm{m/s}$ (b) $\alpha = 0.4°, U = 39\,\mathrm{m/s}$

Figure 3.12: Standard deviation of the hot-wire signals at the wall ($y = 0\,\mathrm{mm}$) under varying flight states, DBD on/off at $T = 13.4\,\mathrm{mN/m}$ ($P = 54.2\,\mathrm{W/m}$).

in Figure 3.12(a), hardly reveal the signal peak at the downstream end of the domain. Here, only the parallel displacement of the trend line slopes Δ_{par} can be compared, rendering the transition delay 2.5%. In order to better resolve the transition process, the angle of attack is decreased leading to increasing flight velocities. A more precise quantification is possible for the decreased $\alpha = 0.4°$, $U = 39\,\mathrm{m/s}$ in Figure 3.12(b). For both the controlled and uncontrolled cases, the transition peak is observed within the measurement area. The displacement of the peak Δ_{peak} and of the slopes both indicate a transition delay of 2%. The trend of diminishing transition delay for lower α is consistent with the decreasing boundary-layer stability due to flow speed and pressure gradient augmentation.

4 Numerical Optimization

Boundary-layer computations using a finite-differences solver as presented by [10] are performed based on an input pressure distribution from *Xfoil*, calculated for the wing glove geometry with the mentioned flow parameters. The laminar boundary-layer code diverges downstream of $x/c = 0.777$ due to the strong pressure gradient imposed by the reflexed trailing edge of the wing glove pressure side, predicting laminar separation. The results of a linear stability analysis of the flow case are depicted in Figure 4.1. It contains a neutral stability curve with the critical

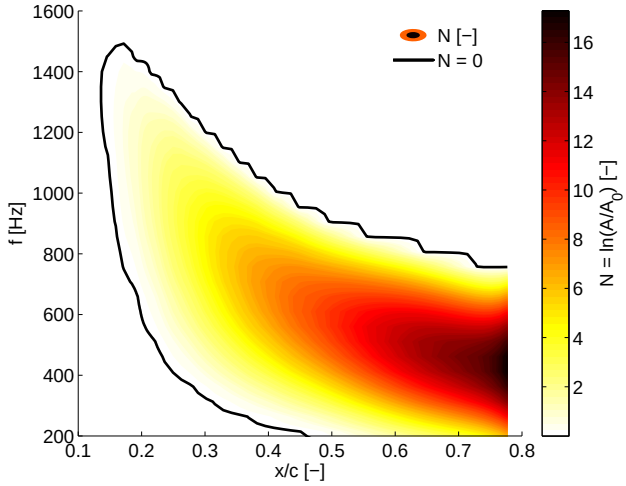

Figure 4.1: Stability diagram of wing glove pressure side, $\alpha = 0.7°$ and $U = 38$ m/s. Contour levels indicate N-factor magnitude, black solid line indicates neutral stability curve.

point at $x/c = 0.12$ for a frequency $f = 1400$ Hz yielding an approximate Reynolds number of $Re_{\text{crit}} = 4.1 \times 10^5$. If a critical N-factor of $N_t = 10$ is assumed to resemble fully turbulent flow (as frequently done in flight investigations), transition is expected at $x/c = 0.485$. The predicted transition location agrees well with the measured values in flight.

The laminar boundary-layer code in connection with an implemented DBD force model and subsequent stability analysis is used to evaluate the impact of actuator positioning at $x/c = 0.33$ on the pressure side of the wing glove airfoil. The N-factor evolution of discrete disturbance frequencies is illustrated in Figure 4.2 (a) without DBD forcing. For comparison, the case of maximized actuator thrusting at $T = 15.6$ mN/m is presented in Figure 4.2 (b). For the flow-control case, the expected critical N-factor $N_t = 10$ is crossed at $x/c = 0.503$, yielding a predicted transition delay of $\Delta x_{\text{trans}}/c = 1.85\%$. Considering the flow speed and the large chord Reynolds number of approximately $Re = 3 \times 10^6$, this transition delay underestimates the values found in the flight experiments.

Since the actuator force field can be arbitrarily positioned along the surface of the investigated body in numerical studies, the sensitivity of the flow stability to a variation of the actuator location can be evaluated. The maximum N-factor at the end of the computational domain is evaluated as a function of the actuator placement. Figure 4.3 illustrates the results of these computations by comparing the maximum N-factors for different actuator positions and thrust magnitudes.

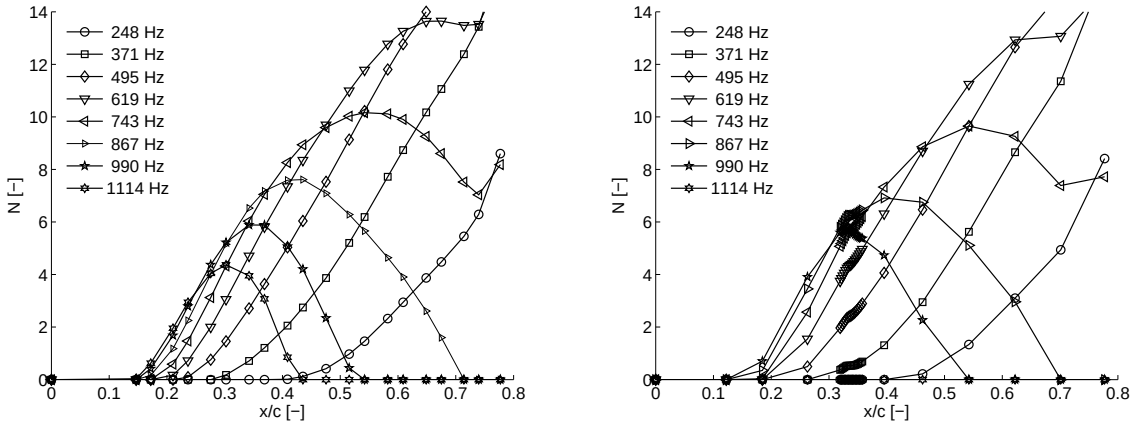

(a) DBD off) (b) DBD on, $T = 15.6\,\text{mN/m}$

Figure 4.2: N-factor evolution of discrete disturbance frequencies (a) without and (b) with DBD thrust $T = 15.6\,\text{mN/m}$.

The results recommend a DBD placement at the location $x/c = 0.25$ where the maximum N-factor is minimized. Table 4.1 summarizes the predicted transition locations $x_{\text{trans}} = x(N_t = 10)$ for DBD actuation at the chosen $x/c = 0.33$ and the optimal $x/c = 0.25$. The results for various thrust magnitudes and equivalent power consumption are listed, facilitating easy comparison of the investigated cases. As the actuator thrust is increased, higher transition-delay predictions

T [mN/m]	P [W/m]	x_{trans}/c	
		$x_{\text{DBD}}/c = 0.33$	$x_{\text{DBD}}/c = 0.25$
0	0.0	0.485	0.485
7.8	3.7	0.488	0.488
9.1	38.1	0.492	0.493
11.3	45.7	0.497	0.498
13.5	55.1	0.503	0.505
15.6	64.4	0.503	0.506

Table 4.1: Comparison of predicted transition locations for varied thrust and two optional DBD actuator locations, $x_{\text{DBD}}/c = 0.33$ and $x_{\text{DBD}}/c = 0.25$.

are observed for both actuator positions. A saturating trend is observed for elevated thrust magnitudes, limiting the possible transition delay. The overall impact on the transition location by changing between the two actuator locations is negligible in comparison to optimizing the actuator thrust.

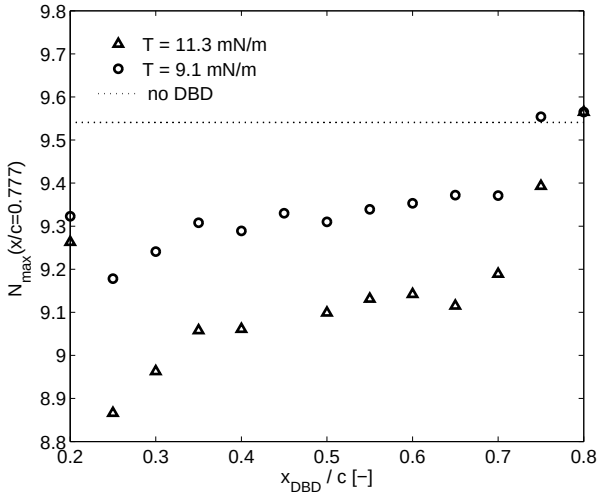

Figure 4.3: Sensitivity of N-factor growth to actuator placement. Maximum N-factor at end of the domain $x/c = 0.777$ for various actuator locations x_{DBD}/c and thrust levels T.

5 Efficiency Estimate

Computational fluid dynamics enables flow simulations deducing all flow quantities of interest. Simple panel methods are sufficient to deliver the lift and drag of airfoils at specified flow conditions. Here, *Xfoil* is employed to simulate the flight conditions on the wing glove at $U = 38\,\mathrm{m/s}$ and $\alpha = 0.7°$. The drag coefficients are derived from two simulations with fixed transition on the pressure side, conservatively representing either the natural transition conditions ($x_{\mathrm{trans}}/c = 0.47$) or the transition location under DBD influence ($x_{\mathrm{trans}}/c = 0.5$). Figure 5.1 illustrates the local skin friction coefficient c_f along the pressure side of the glove with and without flow control. Illustrative, the difference between the area under the particular curves

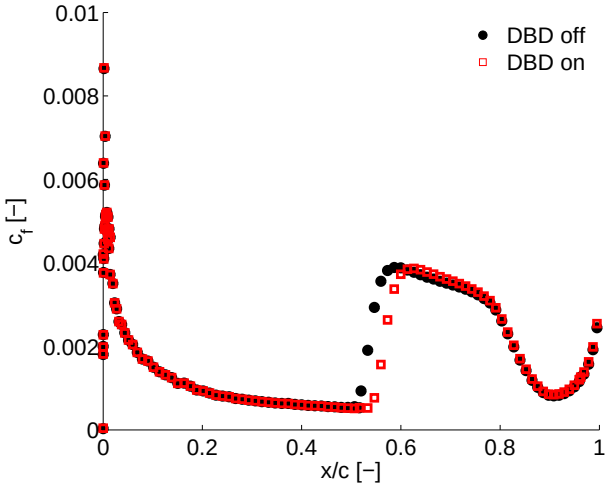

Figure 5.1: Friction coefficient along the glove pressure side derived from *Xfoil* for forced transition locations $x_{\mathrm{trans}}/c = 0.47$ (DBD off, circles) and $x_{\mathrm{trans}}/c = 0.5$ (DBD on, squares).

clarifies the integral effect of 3% transition delay. In both simulated *Xfoil* cases, the pressure drag component is equal such that the drag coefficient reduction is caused only by the friction component, $\Delta c_D = \Delta c_{D,f} = 0.00008$. If these values are processed, a reduction of the necessary propulsion power by $\Delta P_p = 7.34\,\mathrm{W/m}$ is computed. The flow-control efficiency can hence be defined by the ratio of the saved propulsion power ΔP_p to the actuator power consumption P.

$$\eta = \frac{\Delta P_p}{P} \tag{5.1}$$

The power consumed in the flight experiments is closed-loop controlled at $P = 66.6\,\mathrm{W/m}$, yielding an efficiency of $\eta = 11\%$. In the current setting, no net gain is achieved since the power consumption significantly exceeds the power savings which is a typical result encountered in active flow-control experiments. Considering the novelty of the presented experiments and their preliminary nature, the calculated efficiency is close to a revelation. Enhancements of the actuator configurations, materials and optimization of the actuator location renders a net gain plausible in future experiments.

6 Conclusions and Outlook

Two experimental setups have been employed to foster the understanding of DBD transition control mechanisms and to optimize the obtainable transition delay on a flat plate and on a wing glove for flight investigations. Accompanying numerical investigations support the experimental findings and enable parametrical studies for optimization purposes.

Generic flat-plate wind-tunnel experiments demonstrate the control of naturally occurring, TS-wave dominated transition by means of a single DBD actuator. A parametric variation of the actuator number, thrust and positioning indicates a strong dependence of the transition control effectiveness on all these parameters. Increased effectiveness is found for higher forcing magnitudes; however, no flow control optimum is identified at the selected speed of $U_\infty = 20\,\mathrm{m/s}$. The limited momentum induced by the single actuator compared to the freestream momentum restricts the obtainable effect. Due to the danger of dielectric breakdown at excessively high voltages, a limitation of the actuator power is necessary, such that the best achievable transition delay is limited by the actuator performance and not by stability effects. A variation of the actuator position and application of multiple-actuator arrays yields significantly enhanced effectiveness for optimized locations. The conducted experiments insinuate that adequate positioning of an actuator is more important than a multiplication of the force locations which provokes a increase of the total power consumption.

Initial wind-tunnel measurements and following flight tests with a specially designed wing glove demonstrate the possibility to delay naturally occurring transition by means of steadily operated DBD actuators at $Re = 3 \times 10^6$ under varying ambient conditions. The atmospheric conditions and their influence on the DBD power consumption have been thoroughly analyzed, paving the way for a successful implementation of a closed-loop performance controller and enabling constant flow-control authority during measurement flights.

Although the presented effort is not the very first airborne DBD application, compare [15], it is the first and only one to show a desirable flow-control effect under realistic flight conditions. The respectable transition delay of 3% chord length during the first non-optimized flights agrees with initial wind-tunnel measurements and exceeds the expectations from numerical simulations. Both the numerics and the flight experiments indicate a saturation of the control effectiveness despite increasing thrust magnitude, such that an efficiency consideration between the energy expense and savings is necessary. A conservative calculation of the net drag reduction by approximately 1.9% results in a computed power efficiency in the two-digit percentage range, rendering a net benefit plausible if the experimental setup is refined and further optimized.

Future flight experiments could cover a systematic variation of the DBD actuator position to enhance the flow control effectiveness and extend the flight envelope of observable transition delay. A combination of the continuous DBD operation with selective cancelation of boundary-layer instabilities by pulsed actuation is expected to enhance the overall effectiveness at reduced power consumption, thereby approaching the goal of an energetic net gain.

7 Financial status report

Resource	Projected	Spent
Personnel		
Graduate student	94.400$	94.400$
Undergraduate student	4.960$	4.960$
Travel	1.180$	1.180$
Sum	100.540$	100.540$
Materials and Supplies		
Sensors	14.120$	14.120$
Fuel & glider operation costs	8.220	8.220$
Sum	22.340$	22.340$
Total	122.880$	122.880 $

Bibliography

[1] AFOSR Grant FA8655-08-1-3032 final report, TU Darmstadt, August 2011.

[2] Bénard, N., Balcon, N. and Moreau, E. (2008): Electric wind produced by a surface dielectric barrier discharge operating in air at different pressures: aeronautical control insights. *J. Phys. D: Appl. Phys.*, 41(4):042002 (5pp).

[3] Bénard, N., Balcon, N. and Moreau, E. (2009): Electric wind produced by a surface dielectric barrier discharge operating over a wide range of relative humidity. In *47th AIAA Aerospace Sciences Meeting, Orlando, Florida, USA*, AIAA 2009-488.

[4] Bénard, N. and Moreau, E. (2010): Effects of altitude on the electromechanical characteristics of a single dielectric barrier discharge plasma actuator. In *41st Plasmadynamics and Lasers Conference, Chicago, Illinois, USA*, AIAA 2010-4633.

[5] Duchmann, A., Reeh, A., Quadros, R., Kriegseis, J., and Tropea, C. (2010): Linear stability analysis for manipulated boundary-layer flows using plasma actuators. In *Seventh IUTAM Symposium on Laminar-Turbulent Transition*, volume 18 of *IUTAM Bookseries*, pages 153–158. Springer Netherlands, ISBN 978-90-481-3723-7.

[6] Duchmann, A., Kurz, A., Widmann, A., Grundmann, S., and Tropea, C. (2012): Characterization of Tollmien-Schlichting wave damping by DBD plasma actuators using phase-locked PIV. In *50th AIAA Aerospace Sciences Meeting, Nashville, Tennessee, USA*, AIAA 2012-903.

[7] Duchmann, A., Vieira, D., Grundmann, S., and Tropea, C. (2012): Stabilization of laminar boundary-layer flow using dielectric barrier discharges. In *Proc. Appl. Math. Mech.*, volume 11. Wiley.

[8] Duchmann, A. (2012): Boundary-Layer Stabilization with Dielectric Barrier Discharge Plasmas for Free-Flight Application. *Ph.D. Thesis*, Institute of Fluid Mechanics and Aerodynamics, TU Darmstadt.

[9] Grundmann, S. (2008): Transition Control using Dielectric-Barrier Discharge Actuators. *Ph.D. Thesis*, Institute of Fluid Mechanics and Aerodynamics, TU Darmstadt.

[10] Köhler, M. (2011): Development and implementation of a method for solving the laminar boundary layer equations in airfoil flows. *Master Thesis*, TU Darmstadt.

[11] Kriegseis, J. (2011): Performance Characterization and Quantification of Dielectric Barrier Discharge Plasma Actuators. *Ph.D. Thesis*, Institute of Fluid Mechanics and Aerodynamics, TU Darmstadt.

[12] Kriegseis, J., Kurz, A., Duchmann, A., Grundmann, S. and Tropea, C. (2012): Influence of air flow on the performance of DBD plasma actuators. In *50th AIAA Aerospace Sciences Meeting, Nashville, Tennessee, USA*, AIAA 2012-406.

[13] Mack., L.M. (1977): Transition prediction and linear stability theory. *Technical Report CP-224, AGARD Laminar-Turbulent Transition*, 22p.

[14] Séraudie, A., Vermeersch, O., Arnal, D. (2011): DBD plasma actuator effect on a 2D model laminar boundary layer. Transition delay under ionic wind effect. In *29th AIAA Applied Aerodynamics Conference, Honolulu, Hawaii*, AIAA 2011-3515.

[15] Sidorenko, A., Budovsky, A., Pushkarev, A., and Maslov, A. (2008): Flight testing of DBD plasma separation control system. In *46th AIAA Aerospace Sciences Meeting and Exhibit, Reno, Nevada*, AIAA 2008-3731.

[16] Ustinov, M., Kogan, M., Litvinov, V., and Uspensky, A. (2011): Natural laminar-turbulent transition delay by dielectric barrier discharge. *Journal of Physics: Conference Series 318*, 022037.